Torsional Buckling Analysis and Damage Tolerance of Graphite/Epoxy Shafts

O. A. BAUCHAU, T. M. KRAFCHACK AND J. F. HAYES
Department of Mechanical Engineering
Aeronautical Engineering and Mechanics
Rensselaer Polytechnic Institute
Troy, N.Y. 12180-3590

(Received September 16, 1986)
(Revised February 7, 1987)

ABSTRACT

The measured torsional buckling load of Graphite/Epoxy shafts is found in good agreement with theoretical predictions based on a general shell theory that includes elastic coupling effects and transverse shearing deformations. The direction of the applied torque and the lay-up stacking sequence drastically affects the buckling load (up to 80%). Transverse shearing deformations are found significant when the number of circumferential waves in the buckling pattern is larger than 3. The residual strength of shafts with holes is also measured, and the dominant failure mode remains torsional buckling. The buckling mode patterns are seemingly unaffected by damage but buckling loads are lower compared to undamaged specimens. Material failure concentrated around the hole does not occur until the hole size is approximately one-third of the shaft's diameter. Teflon disks inserted between plies to simulate delaminations decrease the buckling load, but not significantly. In conclusion, stiffness characteristics, rather than strength characteristics dominate the behavior of thin-walled, undamaged shafts under torsional load, and this appears to remain true for shafts with sizable damage (up to about one-third of the shaft's diameter).

INTRODUCTION

ADVANCED COMPOSITE MATERIALS seem ideally suited for long, power driveshaft applications. Their elastic properties can be tailored to increase the torque they can carry as well as the rotational speed at which they operate [1,2]. For thin-walled shafts, the failure mode under an applied torque is torsional buckling rather than material failure. On the other hand the rotational speed is limited by lateral stability considerations: most designs are subcritical, i.e. rotational speed must be lower than the first natural bending frequency of the shaft. This frequency is proportional to $\sqrt{(E/\varrho)}$ where E is the longitudinal stiffness modulus of the shaft and ϱ the material density. For lay-ups containing a significant proportion of fibers running along the shaft's axis this ratio can be made larger than for metal shafts resulting in higher natural frequencies. Tapering the wall

0021-9983/88/03 0258–13 $4.50/0

thickness distribution along the span can further increase this frequency [3,4]. Alternatively, a longer unsupported length of shaft can be used for a given rotational speed.

For a realistic driveshaft system, improved lateral stability characteristics must be achieved together with improved torque carrying capabilities. The dominant failure mode, torsional buckling, is strongly dependent on fiber orientation angles and ply stacking sequence. The first goal of this paper is to present a theoretical model of the torsional buckling behavior of circular cylindrical shells made of laminated composites and to validate this model by comparing its predictions with experimental results.

Design studies [1,2] have shown that significant weight savings can be achieved with composite shafts, however their damage tolerance characteristics remain largely unknown. Foreign object damage during maintenance or normal operation, as well as ballistic impact damage present major threats to the drive system. A full assessment of the damage tolerance of drive systems should include ballistic impact tests on loaded, high speed rotating shafts. However, considering the difficulty and the very large number of parameters involved in such a test, it was felt appropriate for a preliminary study to concentrate on a simpler problem, namely the residual torsional strength of shafts with damage. The second goal of this paper is to present such experimental results for two limiting types of damage: circular holes of various diameter (as would result from a high velocity impact), and imbedded delaminations (resulting from a non-penetrating impact).

SPECIMEN FABRICATION

Circular cylindrical specimens were fabricated from 6, 8, or 10 layers of prepreg wrapped around an aluminum mandrel. The prepreg consists of Union Carbide's T-300 graphite fibers in Fiberite's 948A1 low temperature curing epoxy. Specimens were vacuum bagged and cured in an autoclave under a 94 psi pressure. The curing cycle consists of a 30 minute hold at the resin flow temperature (130°F), followed by a two hour cure at 250°F. Table 1 summarizes the lay-

Table 1. Lay-up (starting from innermost ply) and geometry of the specimens.

	Lay-up Definition	*L* [m]	*R* [mm]	Number of Specimens
L#1	15, −15, −45, −15,15,45	0.260	41.27	4
L#2	45,15, −15, −45, −15,15	0.260	41.27	4
L#3	−45, −15,15,45,15, −15	0.260	41.27	4
L#4	15, −15,15, −15,15, −15	0.330	37.33	6
L#5	30, −30,30, −30,30, −30	0.320	37.19	6
L#6	45, −45,45, −45,45, −45	0.320	37.42	6
L#7	0_2,45, −45,45, −45,0_2	0.320	37.42	4
L#8	0_2,45,0, −45,0,45, −45	0.320	46.86	5
L#9	0_2,45,0_2, −45,0_2,45, −45	0.320	46.90	4

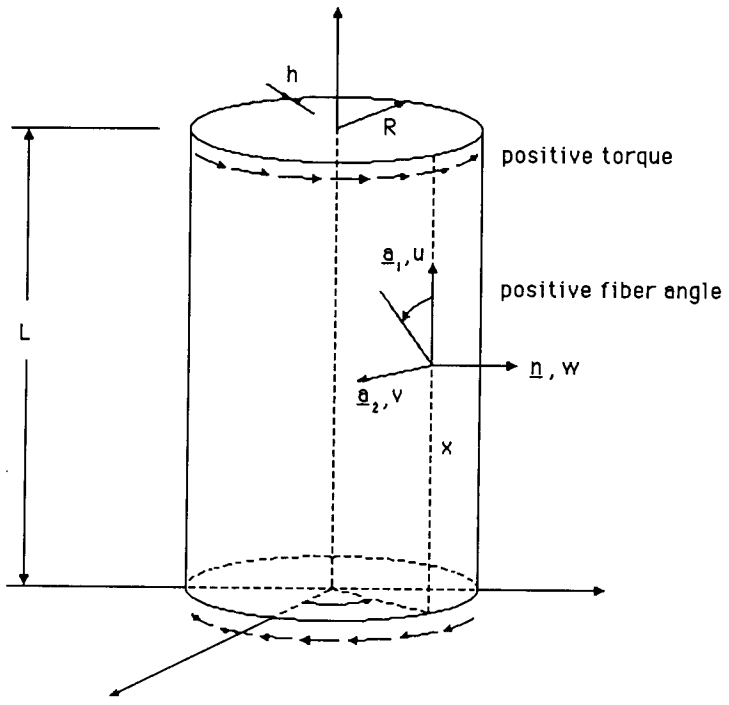

Figure 1. *Sign conventions and geometry of the shell.*

up (starting from the innermost ply, 0° is along the axis of the shaft and positive angles are defined in Figure 1), the mean radius R, the length L, and the number of specimens tested in each group. Static torsional tests were conducted in a MTS servohydraulic testing machine at a constant twist rate of one degree per minute. The resulting shear strain rate was typically 40 microstrain/sec. End attachments consist of aluminum plugs which fit tightly inside both ends of each tube. The specimen is bolted onto these plugs by means of eight equally spaced bolts and washers are used to distribute the clamping pressure. To avoid stress concentration and premature failure at the bolted connection the tubes were reinforced with ±45° layers over a 3cm zone at both ends. In these reinforced zones the wall thickness was doubled. Figure 3 shows the specimen configuration.

The stiffness properties of this material were obtained for tensile coupons in an independent effort [5] as $E_L = 134$ GPa, $E_T = 8.5$ GPa, $G_{LT} = G_{13} = 4.6$ GPa, $G_{23} = 4$ GPa, $\nu_{LT} = 0.29$, and the ply thickness is 133.4 10^{-6} m.

TORSIONAL BUCKLING MODEL

A general treatment of buckling of anisotropic cylinders under combined loading with arbitrary boundary conditions was presented by Cheng and Ho [6,7].

Their development is based on Flügge's linear shell theory and requires considerable numerical analysis to obtain critical loads. An extensive study on the buckling of filament wound Glass/Epoxy cylinders was undertaken by Holston [8] and the experimental torsional buckling loads were found in poor agreement with theoretical predictions of Reference [6] and [7]. A more recent study by Wilkins and Love [9] on Graphite and Boron/Epoxy cylinders also reported considerable disagreement between experimental and predicted torsional buckling loads. Finally, Tennyson [10] found good agreement between the torsional buckling loads of Glass/Epoxy tape-wound cylinders and predictions based on the linearized Donnell equations.

In view of these conflicting reports, a model of the torsional buckling behavior of circular cylinders was developed based on a general shell theory. In the derivation of the equations special care was taken to properly model the specific characteristics of laminated shafts: elastic coupling effects as well as transverse shearing deformations were taken into account and the usual simplifying assumptions (such as Donnell's or Flügge's assumptions) were not made.

The in-plane strain components $\underline{\epsilon}^T = (\epsilon_{11}, \epsilon_{22}, \epsilon_{12})$, and the transverse shearing components $\underline{\gamma}^T = (\gamma_{13}, \gamma_{23})$ are

$$\epsilon_{11} = (l_{11} + \zeta m_{11}) + \frac{1}{2}(l_{11}^2 + l_{21}^2 + l_{31}^2)$$

$$\epsilon_{22} = \frac{(l_{11} + \zeta m_{22})}{(1 + \zeta/R)} + \frac{1}{2(1 + \zeta/R)^2}(l_{12}^2 + l_{22}^2 + l_{32}^2) \tag{1}$$

$$\epsilon_{12} = \frac{(l_{12} + \zeta m_{12})}{(1 + \zeta/R)} + l_{21} + \zeta m_{21} + \frac{1}{(1 + \zeta/R)}(l_{12}l_{11} + l_{21}l_{22} + l_{31}l_{32})$$

$$\gamma_{13} = \phi_1 + l_{31} \tag{2}$$

$$\gamma_{23} = \frac{\phi_2 + l_{32}}{(1 + \zeta/R)}$$

where

$$l_{11} = u', \quad l_{21} = v', \quad l_{31} = w' \tag{3}$$

$$l_{12} = \mathring{u}/R, \quad l_{22} = (\mathring{v} + w)/R, \quad l_{32} = (\mathring{w} - v)/R$$

$$m_{11} = \phi_1', \quad m_{21} = \phi_2' \tag{4}$$

$$m_{12} = \phi_1^\circ/R, \quad m_{22} = \phi_2^\circ/R, \quad m_{33} = -\phi_2/R$$

The notations $(\,)'$ and $(\,)^\circ$ represent the partial derivatives with respect to the variables x and θ, respectively, as defined in Figure 1; u, v, and w are the three

displacement components measured along the local axes; ϕ_1 and ϕ_2 are the rotations (about $\underline{a}_1$ and $\underline{a}_2$, respectively) of the normal to the midplane, which are independent of the slope of the shell since shearing deformations are taken into account. The strain expressions (1) and (2) are used to evaluate the strain energy U,

$$U = \tfrac{1}{2} \int_S \int_\zeta (\underline{\epsilon}^T[Q]\underline{\epsilon} + \underline{\gamma}^T[Q_s]\underline{\gamma})\, d\zeta\, dS \tag{5}$$

where $[Q]$ is the inplane stiffness matrix, $[Q_s]$ the transverse shear stiffness matrix, S the midplane surface of the shell, and ζ the through-the-thickness variable. Equation (5) can be integrated over the thickness of the shell; in this process the stiffness of each individual ply is used and all the elastic couplings are accounted for in a rational fashion.

The five unknown functions of the problem are now represented as series expansions. Trigonometric functions are assumed in the circumferential direction to yield

$$a(x,\theta) = \sum_{k=1,N} (C_a^k \cos n\theta + S_a^k \sin n\theta)\, f_a^k(x) \tag{6}$$

where $a(x,\theta)$ represents any one of the unknown functions u, v, w, ϕ_1, or ϕ_2; n is the circumferential wave number and N the number of functions $f_a^k(x)$ used to represent the axial dependency of the solution. If both ends of the tube are clamped all the displacement components must vanish at $x = 0$ and L and a reasonable choice for the functions f_a^k is

$$f_a^k(x) = \sin k\pi x/L \tag{7}$$

For simply supported ends all displacement components must vanish at $x = 0$ and L except for the rotation ϕ_1 which is arbitrary. Hence all functions were selected as in (7) except for

$$f_{a_1}^k(x) = \cos k\pi x/L \tag{8}$$

The integration over the surface of the shell is now readily performed to yield an expression for the strain energy U that is only dependent on the unknown coefficients C_a^k and S_a^k. The remaining steps of the formulation follow usual buckling calculation procedures [11], and the buckling load is obtained as the lowest eigenvalue of a standard eigenproblem.

TORSIONAL BUCKLING BEHAVIOR

Table 2 lists the experimentally measured buckling torques T_{cr}, their experimental coefficients of variation, and the critical shearing stresses $\tau_{cr} = T_{cr}/2\pi R^2 h$ (h is the wall thickness) for the various specimens; each critical load is an average of 4 to 6 tests. For each experiment, the torque-twist curve was recorded (load-cell torque versus cross-head twist) and buckling was detected by a sharp decrease in this curve. Typical torque-twist curves for L#1 and L#2 are shown in Figure 2. The buckling pattern consists of helical waves winding around the cylinder as shown in Figure 3. These helical waves were equally spaced over the circumference of the shaft and the number of circumferential waves n is also reported in Table 2. No fiber or matrix failure was apparent at buckling; in fact, some specimens were tested repeatedly up to buckling and nearly identical buckling loads were obtained each time. Since the tests were run under stroke control it was possible to trace the behavior of the samples well past the buckling load (see Figure 2), however, the applied load continuously decreased after buckling. In other words, no post-buckling strength was observed, and had the experiment been run under torque control, catastrophic collapse of the tube would have occurred at buckling. Under stroke control as in the present experiment, material failure and a total collapse of the tube only occurred for very large twists, equal to several times the twist at buckling.

Table 2 also lists the theoretical predictions for the torsional buckling of cylinders with clamped and simply supported edges, according to the model described in the previous section. Theoretical predictions are found in good agreement with experimental measurements, except for lay-up L#5 where theory overpredicts the buckling load by about 40%. In all cases the experimentally observed number of circumferential waves was equal to the predicted number. In the experimental set-up the boundary condition was neither clamped nor simply supported, however theoretical prediction for simply supported edges are in slightly better agreement with experimental results (about 4% average error versus 6% for clamped edges). Theoretical predictions were in general slightly higher than measurements.

It is interesting to note that lay-ups L#1 and L#2 have the same number of plies and ply orientations, but different stacking sequences. In fact L#1 and L#2 have

Table 2. Comparison of measured buckling torques T_{cr} [N.m], coefficients of variation C.V. [%], and stresses τ_{cr} [Mpa] with theoretical prediction for clamped and simply supported edges.

	Experimental			Prediction	Prediction
	T_{cr} (C.V.)	τ_{cr}	n	Clamped Edges	Simply Supported
L#1	486 (4.0%)	56	5	541 (11%)	523 (7.6%)
L#2	655 (3.4%)	75	5	733 (12%)	712 (8.7%)
L#3	350 (3.4%)	40	5	379 (8%)	366 (4.5%)
L#4	330 (3.0%)	46	5	355 (7.6%)	349 (5.8%)
L#5	390 (9.0%)	55	4	540 (38%)	535 (37%)
L#6	490 (5.0%)	68	4	495 (1%)	490 (0%)
L#7	543 (16.0%)	56	4	557 (2.5%)	540 (−0.5%)
L#8	1575 (9.0%)	105	4	1562 (−0.8%)	1544 (−2%)
L#9	2400 (10.0%)	127	4	2543 (6%)	2491 (3.8%)

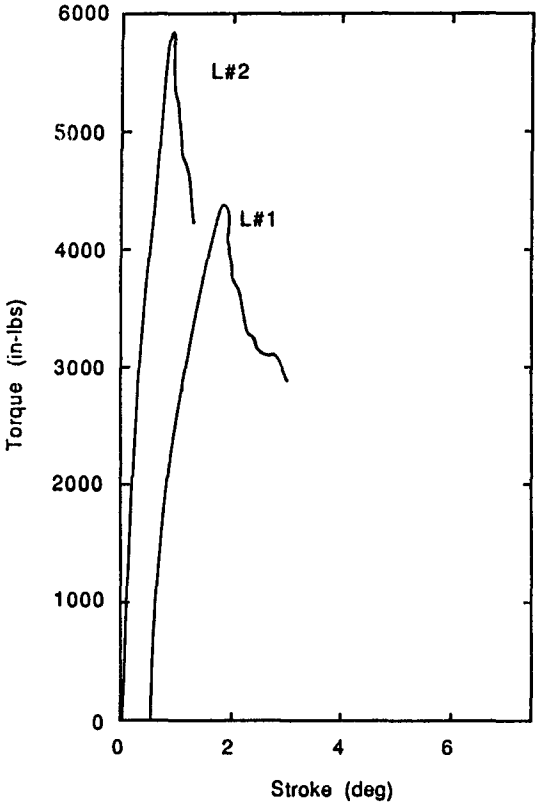

Figure 2. *Typical torque-twist curves for L#1 and L#2.*

identical inplane stiffness matrices A [12], identical bending stiffness matrices D, and their coupling stiffness matrices B are of identical magnitude but opposite signs. The B matrix appears to have a destabilizing effect in the first case whereas in the latter case, the change of sign has a stabilizing effect. This results in a 30% increase in buckling stress from 56 to 75 Mpa. The same observation is true for L#7 and L#8 where the stacking sequence effect is about 80% from 56 to 105 Mpa (in this case the matrices B and D are different for the two lay-ups).

Consider now L#2 and L#3, the results for these two lay-ups were actually obtained with the same specimen type, but the torque was applied in opposite directions. For consistency, all the results in Table 2 are for positive torques, as defined in Figure 1. A negative torque applied on L#2 was treated as a positive torque on L#3, where L#3 has the same orientation angles as L#2 but opposite signs (Table 1). The direction of the applied torque appears to be very important and the buckling stresses show an 80% difference from 40 to 75 Mpa. Here again this effect can be related to the coupling stiffness matrix B.

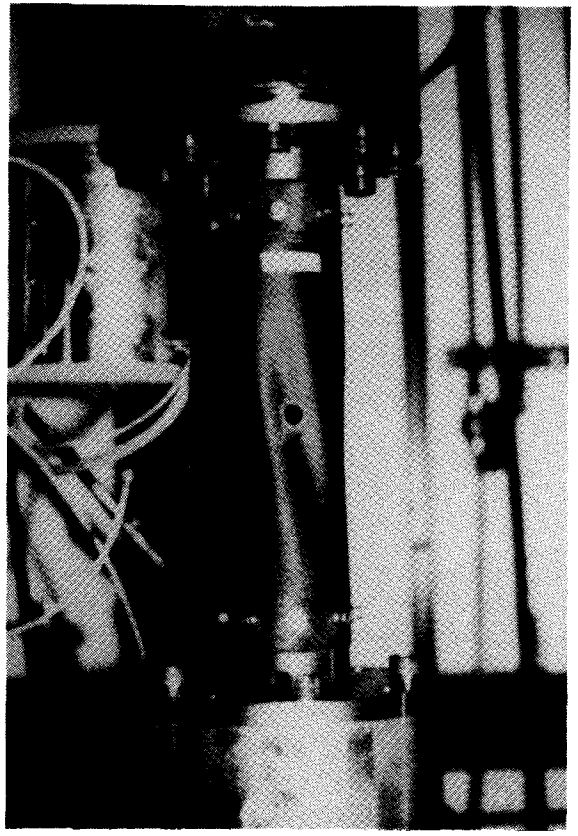

Figure 3. *Typical buckling pattern for specimen L#1 with 12.7 mm diameter hole.*

Finally the case of lay-up L#5 calls for some additional comments. In two References [13,14] Lagace proposed a Ply Buckling Model pertinent to the buckling analysis of laminated cylinders under compressive axial load. In this model the outermost ply of the tube is assumed to buckle prematurely because of initial imperfections in the manufacturing (such as voids, eccentricities, etc.) and because it is less constrained than inner plies. Hence the load carrying capability of this buckled outer ply can be neglected, and the final buckling load of the tube can be obtained by considering the inner plies only. If this model is applied to the present torsional buckling problem, the critical torque for L#5 could be obtained considering the lay-up $30, -30, 30, -30, 30°$. For this configuration the calculated buckling loads are 408 and 390 N.m for the clamped and simply supported cases respectively, which appears to be in close agreement with the experimental value of 390 N.m. However, a visual examination of the L#5 specimens after buckling did not reveal any evidence of outer ply buckling and the failure mode of these

Table 3. Transverse shearing effect on buckling load.

L [m]	Buckling Torque [N.m] *No* Shearing Effects	Buckling Torque [N.m] *With* Shearing Effects	Number of Circf. Waves *n*
0.260	569 (5.2%)	541	5
0.510	380 (4.7%)	363	4
1.010	244 (0.1%)	243.9	3
2.540	143 (0.0%)	143	2
5.080	117 (0.0%)	117	2

tubes did not appear different from that of any other specimen type. Application of the Ply Buckling Model to the other lay-ups of this study yielded very poor correlation with experimental results. Hence this model does not seem to be appropriate for modeling the torsional buckling behavior of tubes, and the good correlation obtained with L#5 might be fortuitous.

The importance of transverse shearing effects was assessed in a numerical study: Table 3 lists the calculated buckling loads with, and without shearing effects for various lengths of shaft (the lay-up is L#1). For the tested configuration ($L = 0.260$ m), shearing effects lowered the buckling load by about 5%. When the shaft's length increases, the buckling pattern presents a decreasing number of circumferential waves, and the shearing effect becomes less and less significant (for $n \leq 3$ they are negligible). It is however interesting to note that when $n > 3$ shearing effects can be significant even for very thin laminated shells (in this case $R/h > 50$).

Various theories are found in the literature such as Donnell's or Flügge's theories [15]. These models all make an assumption about the ratio h/R. Donnell's theory neglects h/R with respect to unity whereas Flügge's model keeps terms up to $(h/R)^2$. These assumptions are made to simplify the integration through the thickness of the shell. In this effort no such simplification was made. Table 4 compares the buckling load of L#1 obtained with the Donnell assumption and with exact integration. As the length of the shaft increases the difference tends to increase, but remains small even when $n = 2$. This means that Donnell or Flügge's assumption are valid even for the analysis of long, thin-walled driveshafts.

Table 4. Effect of theory type on buckling load.

L [m]	Buckling Torque [N.m] Donnell Theory	Buckling Torque [N.m] Exact Integration	Number of Circf. Waves *n*
0.260	543 (0.4%)	541	5
0.510	365 (0.6%)	363	4
1.010	246 (0.8%)	244	3
2.540	146 (2.0%)	143	2
5.080	119 (2.0%)	117	2

Finally an attempt was made at deriving a simplified solution to predict the torsional buckling load for very long shafts. The resulting procedure could not be put into a closed form, and was extremely inaccurate when compared to the present solution. In fact even when $n = 2$ the buckling load remains strongly dependent on the shaft's length, as shown in Table 3. Hence the "infinite length" assumption necessary to simplify the solution procedure does not yield reliable results; this contrasts with isotropic shells for which this assumption yields good results for comparable L/R ratios.

DAMAGE TOLERANCE BEHAVIOR

A damage tolerance study was conducted on specimens with lay-ups L#1 and L#2. These configuration were selected as they appear to be realistic candidates for helicopter drive shafts applications [1,2]. Circular holes were drilled in the specimens with a carbide tip drill and a wooden plug was inserted inside the tube during the drilling operation. Holes of four different sizes were considered: 6.35, 12.7, 19.05, and 25.4 mm in diameter. The residual strength of these damaged specimens was measured by means of a static torsional test conducted at a constant twist rate. Table 5 summarizes the failure loads for the various configurations (the average of four tests is reported for each category, as well as the coefficient of variation).

For all hole sizes, except 25.4 mm, the observed failure mode remains torsional buckling and was detected by a sharp decrease in the torque-twist curve. The typical buckling wave pattern remained seemingly unaffected by damage, however the buckling load was lower than for virgin specimens. Tubes with two

Table 5. Failure loads, coefficients of variation C.V. [%], and failure modes for L#1 and L#2 with various diameter holes D [mm].

Hole Diameter	Failure Load (C.V.)	Failure Mode
L#1		
$D = 0.0$	486 (4.0%)	buckling
$D = 12.7$	486 (4.5%)	buckling
Two Holes $D = 12.7$	470 (5.3%)	buckling
$D = 19.05$	400 (5.0%)	buckling
$D = 25.4$	350 (3.0%)	material failure
L#2		
$D = 0.0$	655 (3.4%)	buckling
$D = 6.35$	655 (5.4%)	buckling
$D = 12.7$	550 (7.2%)	buckling
Two holes $D = 12.7$	530 (6.4%)	buckling
$D = 19.05$	460 (5.2%)	buckling
$D = 25.4$	360 (7.0%)	material failure
One delam. $D = 25.4$	610 (3.0%)	buckling
Three delam. $D = 25.4$	600 (4.5%)	buckling

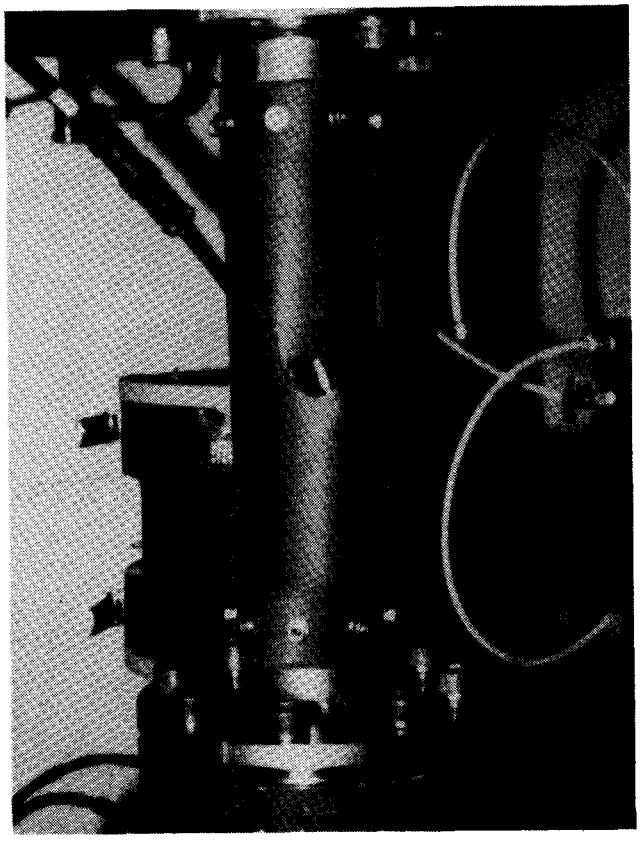

Figure 4. *Typical failure mode for specimen L#2 with 25.4 mm diameter hole.*

diametrically opposed holes of 12.7 mm were also tested. It is interesting to note that nearly identical buckling loads were obtained for one or two holes: 485 versus 470 N.m (or 3.1% decrease) for L#1, and 550 vs. 530 N.m (3.7% decrease) for L#2. Here again the presence of two holes did not seem to affect the overall buckling pattern and no interaction between the holes was apparent.

Specimens with a 25.4 mm diameter hole exhibited a completely different failure mode: the previously described buckling pattern was not observed, but instead, sudden massive failure occurred around the hole involving through-the-thickness cracks and extensive delamination (see Figure 4). It is important to note that this failure mode did not take place until the damage size reached approximately one-third of the shaft's diameter. Nearly identical failure loads were obtained for L#1 and L#2 as should be expected since both configurations only differ in their stacking sequence which has little effect on material failure in this case.

Finally two additional tests were performed on specimens L#1 and L#2 with delaminations. The purpose of these tests is to assess the effect of a blunt object impact on the shaft that could create delamination without a through-the-thickness crack. A delamination was obtained by inserting a 25.4 mm diameter Teflon disk between plies during the manufacturing process. A first test was conducted with one delamination between the outermost ply and the rest of the laminate, whereas in a second test three delaminations were present between the three outermost plies. Torsional buckling was the observed failure mode and the buckling pattern was again unaffected by damage. Once overall buckling occurred, the outer ply buckled out at the location of the Teflon insert. No delamination growth was observed, and the buckling load was reduced by about 7 or 8% as compared to virgin samples.

CONCLUSIONS

Experimentally measured torsional buckling loads of Graphite/Epoxy shafts have been compared with theoretical predictions based on a model that includes elastic coupling effects and transverse shearing deformations. The following conclusions stem from this study:

1. Good agreement is found between measured buckling loads and their theoretical counterparts. Predictions tend to slightly overestimate critical loads.
2. Even for very thin laminated shells ($R/h > 50$), transverse shearing deformations are important when the number of circumferential waves is larger than three.
3. Torque direction and stacking sequence can drastically affect critical loads (up to 80% was experimentally observed).

The damage tolerance study presented in this paper is very preliminary as it deals with residual strength of tubes with holes rather than actual ballistic impact on high speed rotating shafts. However, it calls for the following conclusions:

1. The dominant failure mechanism for torsionally loaded shafts with circular holes is torsional buckling. Material failure did not occur until the damage size reached approximately one-third of the shaft's diameter.
2. Delamination of the outermost plies decreases the buckling load of the shaft, but not significantly.
3. Stiffness characteristics, rather than strength characteristics appear to dominate the behavior of thin walled shafts under torsional load.

If validated by further testing this latter conclusion should have an important impact on the design and material selection for high speed driveshaft applications.

ACKNOWLEDGEMENTS

This research was sponsored by the Army Research Office under Grant DAAG 29-82-k-0093, Dr. Robert Singleton is contract monitor.

REFERENCES

1. Lim, J. W. and M. S. Darlow. "Optimal Sizing of Composite Power Transmission Shafting," *J. Amer. Helic. Soc.*, 31(1):75–83 (January 1986).
2. Lim, J. W. "The Optimal Design of Composite Drive Shafts," Rensselaer Polytechnic Institute, Master Thesis (July 1984).
3. Bauchau, O. A. "Optimal Design of High Speed Rotating Graphite/Epoxy Shafts," *J. Comp. Mat.*, 17:170–181 (March 1983).
4. Bauchau, O. A. "Design, Manufacturing, and Testing of High Speed Rotating Graphite/Epoxy Shafts," Massachusetts Institute of Technology, Ph.D. Thesis (June 1981).
5. Hu, G. S. "Improvements in the Strength Prediction of Notched Composites," Rensselaer Polytechnic Institute, Ph.D. Thesis (June 1985).
6. Cheng, S. and B. P. Ho. "Stability of Heterogeneous Aleotropic Cylindrical Shells Under Combined Loading," *AIAA Journal*, 1(4):892–898 (April 1963).
7. Ho, B. P. and S. Cheng. "Some Problems in Stability of Heterogeneous Aleotropic Cylindrical Shells Under Combined Loading," *AIAA Journal*, 1(7):1603–1606 (July 1963).
8. Holston, A., A. Feldman and D. A. Stang. "Stability of Filament-Wound Cylinders Under Combined Loading," USAF, WPAFB, Techn. Report AFFDL-TR-67-55 (May 1967).
9. Wilkins, D. J. and T. S. Love. "Combined Compression-Torsion Buckling Tests of Laminated Composite Cylindrical Shells," Presented at the 15th AIAA Structures, Structural Dynamics and Materials Conference, Las Vegas (April 1974).
10. Tennyson, R. C. "Buckling of Laminated Composite Cylinders: A Review," *Composites*, pp. 17–24 (January 1975).
11. Timoshenko, S. P. and J. M Gere. *Theory of Elastic Stability*. McGraw-Hill Book Co. (1961).
12. Tsai, S. W. and H. T. Hahn. *Introduction to Composite Materials*. Lancaster, PA:Technomic Publishing Co., Inc. (1980).
13. Lagace, P. A. "Static Tensile Fracture of Graphite/Epoxy," Massachusetts Institute of Technology, Ph.D. Thesis (April 1982).
14. Vizzini, A. J. and P. A. Lagace. "The Role of Ply Buckling in the Compressive Failure of Graphite/Epoxy Tubes," *AIAA Journal*, 23(11):1791–1797 (November 1985).
15. Flügge, W. *Stresses in Shells*. Springer-Verlag (1973).

On Laminate Configurations for Simultaneous Failure

HISAO FUKUNAGA
National Aerospace Laboratory
7-44-1 Jindaiji-higashi
Chofu, Tokyo 182
JAPAN

TSU-WEI CHOU
Center for Composite Materials and Mechanical Engineering Department
University of Delaware
Newark, DE 19716
USA

(Received September 3, 1986)
(Revised January 22, 1987)

ABSTRACT

A particular class of laminated composites is presented where all layers fail simultaneously. Lamiante configurations and loading conditions for simultaneous failure are obtained for laminated composites under in-plane loads.

The present paper also shows the optimal laminate configurations to maximize the in-plane strength for graphite/epoxy composites. Tsai-Wu criterion is used as a first ply failure strength criterion. The particular failure strength characteristics are shown for graphite/epoxy composites.

The strength characteristics of the laminate configurations for simultaneous failure are compared with those of the optimal ones. It is shown that the laminate configurations for simultaneous failure are optimal only for a special loading condition.

1. INTRODUCTION

THE FAILURE STRENGTH characteristics of a laminated composite depend highly on the fiber directions of the individual plies. Thus, it is important to tailor laminate configurations for enhancing the strength of composite structures. Some research works have been made on the failure strength optimization of laminated composites [1–4]. Chao et al. [1] have analyzed the optimal fiber directions of angle-ply laminated cylindrical shells under combined loadings. Ikegami et al. [2] have obtained the optimal fiber directions of $[\theta_1/\theta_2]$ laminates under combined loadings. Donaldson [3] and Wurzel [4] have developed the simplified design

0021-9983/88/03 0271–16 $4.50/0